IJMMM International Journal of Minerals, Metallurgy and Materials 矿物冶金与材料学报（英文版）

Cu^{2+}-catalyzed mechanism in oxygen-pressure acid leaching of artificial sphalerite

Lei Tian, Ao Gong, Xuan-gao Wu, Yan Liu, Zhi-feng Xu, and Ting-an Zhang

Cite this article as:
Lei Tian, Ao Gong, Xuan-gao Wu, Yan Liu, Zhi-feng Xu, and Ting-an Zhang, Cu^{2+}-catalyzed mechanism in oxygen-pressure acid leaching of artificial sphalerite, *Int. J. Miner. Metall. Mater.*, 27(2020), No. 7, pp. 910-923. https://doi.org/10.1007/s12613-019-1918-2

Articles you may be interested in

Hendrik Setiawan, Himawan Tri Bayu Murti Petrus, and Indra Perdana, Reaction kinetics modeling for lithium and cobalt recovery from spent lithium-ion batteries using acetic acid, *Int. J. Miner. Metall. Mater.*, 26(2019), No. 1, pp. 98-107. https://doi.org/10.1007/s12613-019-1713-0

Zhi-yu Chang, Ping Wang, Jian-liang Zhang, Ke-xin Jiao, Yue-qiang Zhang, and Zheng-jian Liu, Effect of CO_2 and H_2O on gasification dissolution and deep reaction of coke, *Int. J. Miner. Metall. Mater.*, 25(2018), No. 12, pp. 1402-1411. https://doi.org/10.1007/s12613-018-1694-4

Evgeniy Nikolaevich Selivanov, Kirill Vladimirovich Pikulin, Lyudmila Ivanovna Galkova, Roza Iosifovna Gulyaeva, and Sofia Aleksandrovna Petrova, Kinetics and mechanism of natural wolframite interactions with sodium carbonate, *Int. J. Miner. Metall. Mater.*, 26(2019), No. 11, pp. 1364-1371. https://doi.org/10.1007/s12613-019-1857-y

Cui Wang, Jian-liang Zhang, Guang-wei Wang, Ke-xin Jiao, Zheng-jian Liu, and Kuo-chih Chou, Combustion characteristics and kinetics of anthracite with added chlorine, *Int. J. Miner. Metall. Mater.*, 24(2017), No. 7, pp. 745-755. https://doi.org/10.1007/s12613-017-1458-6

Hong-pan Liu, Xiao-feng Huang, Li-ping Ma, Dan-li Chen, Zhi-biao Shang, and Ming Jiang, Effect of Fe_2O_3 on the crystallization behavior of glass-ceramics produced from naturally cooled yellow phosphorus furnace slag, *Int. J. Miner. Metall. Mater.*, 24(2017), No. 3, pp. 316-323. https://doi.org/10.1007/s12613-017-1410-9

Saman Beikzadeh Noei, Saeed Sheibani, Fereshteh Rashchi, and Seyed Mohammad Javad Mirazimi, Kinetic modeling of copper bioleaching from low-grade ore from the Shahrbabak Copper Complex, *Int. J. Miner. Metall. Mater.*, 24(2017), No. 6, pp. 611-620. https://doi.org/10.1007/s12613-017-1443-0

IJMMM WeChat

QQ author group

International Journal of Minerals, Metallurgy and Materials
Volume 27, Number 7, July 2020, Page 910
https://doi.org/10.1007/s12613-019-1918-2

Cu^{2+}-catalyzed mechanism in oxygen-pressure acid leaching of artificial sphalerite

Lei Tian[1,2,3], *Ao Gong*[1], *Xuan-gao Wu*[1], *Yan Liu*[4], *Zhi-feng Xu*[1], *and Ting-an Zhang*[4]

1) Institute of Green Metallurgy and Process Intensification, Jiangxi University of Science and Technology, Ganzhou 341000, China
2) Guangdong Institute of Resources Comprehensive Utilization, Guangzhou 510000, China
3) State Key Laboratory of Rare Metals Separation and Comprehensive Utilization, Guangzhou 510000, China
4) Key Laboratory for Ecological Utilization of Multimetallic Mineral, Ministry of Education, Northeastern University, Liaoning 110819, China
(Received: 14 July 2019; revised: 10 September 2019; accepted: 12 September 2019)

Abstract: The potential autoclave was used to study the catalytic mechanism of Cu^{2+} during the oxygen pressure leaching process of artificial sphalerite. By studying the potential change of the system at different temperatures and the SEM–EDS difference of the leaching residues, it was found that in the temperature range of 363–423 K, the internal Cu^{2+} formed a CuS deposit on the surface of sphalerite, which hindered the leaching reaction, resulting in a zinc leaching rate of only 51.04%. When the temperature exceeds 463 K, the system potential increases steadily. The increase in temperature leads to the dissolution of the CuS, which is beneficial to the circulation catalysis of Cu^{2+}. At this time, the leaching rate of Zn exceeds 95%. In addition, the leaching kinetics equations at 363–423 and 423–483 K were established. The activation energy of zinc leaching at 363–423 and 423–483 K is 38.66 and 36.25 kJ/mol, respectively, and the leaching process is controlled by surface chemical reactions.

Keywords: sphalerite; electric potential autoclave; copper(II) ions catalyst; kinetics; activation energy; apparent reaction order

1. Introduction

Sphalerite, the most significant ore in zinc, has a covalent bond lattice structure, and its solubility is very low; thus, the O_2-pressure leaching of sphalerite has very slow kinetics [1–4]. However, with the addition of a suitable catalyst, the leaching efficiency can be significantly improved [5–7]. Sphalerite is a typical sulfide ore and most sulfide minerals are semiconductors, and pressure leaching is essentially an electrochemical reaction process [8–9]. Li *et al.* [10] indicated that defects and impurities in the crystal lattice of sphalerite significantly affect the kinetics of the electrochemical processes, so it is very important for the role of impurities in solid solutions (including mineral phases and ions) on the leaching process.

Under normal circumstances, the concentrates and diffusion rates of Fe^{2+}, Cu^{2+}, and Mn^{2+} in solution determine the leaching rate of Zn. These ions can be assumed to not only function as O_2-carrying materials, but also to participate in the formation of the original battery, functioning as catalysts and oxidants [11–15], promoting the leaching of the valence metal. Under the condition of sufficient O_2 and acidity, Fe^{2+}, Cu^{2+}, Mn^{2+}, and other cations reach a dynamic balance in the reaction system.

Many researchers have investigated the catalysis of different types of metal ions on the leaching of sulfide minerals [16–18]. Ghosh *et al.* [19] used Cu^{2+} as an oxidation catalyst to study the leaching kinetics of sphalerite in ammonia. The results have shown that the surface reaction was the reaction-controlling step, and the apparent activation energy was about 48.3 $kJ \cdot mol^{-1}$, and apparent reaction orders of 0.2, 0.3, and 0.3 were obtained for the oxygen partial pressure, concentrate of ammonia, and Cu^{2+} concentration, respectively. The catalytic action of Cu^{2+} has been attributed to the redox couple Cu^{2+}/Cu^{+}. Ballester *et al.* [20] investigated the catalytic effect of Cu^{2+} on the leaching of sphalerite. In the absence of Cu^{2+}, the oxidative leaching of sphalerite is slow because of the dense layer of elemental S that forms on the mineral surface. However, in the presence of Cu^{2+}, the leaching solution has a higher electrical conductivity, which accelerates the dissolution of the valuable metals.

Several mechanisms for explaining catalytic activity have

Corresponding authors: Zhi-feng Xu E-mail: xzf_1@163.com; Ting-an Zhang E-mail: zta2000@163.net

been proposed. One mechanism is thought to be due to changes in surface reactivity, while the other proposes copper ions as "oxygen carriers" to transfer electrons from S to oxidants. The mechanism and electrochemistry of sphalerite pressure leaching in the Cu^{2+} catalyst system needs further investigation. In this study, the catalytic effect of a Cu^{2+} catalyst system on the dissolution of sphalerite was investigated using a potential autoclave. Experiments were performed to elucidate the catalytic mechanism and the potential-variation rule of the leaching system, and the kinetic influences of several variables on the pressure-leaching process were considered. The research in this paper should be beneficial toward improving the recovery of valuable metals from sphalerite and developing appropriate methods for achieving the effective use of complex sulfide minerals.

2. Experimental

2.1. Materials

Zinc sulfide in sphalerite is α-type; therefore, to obtain artificial sphalerite (α-ZnS), analytical reagent (β-ZnS) was placed in a high-temperature pipe furnace. The preparation of α-ZnS was conducted in an inert-gas atmosphere. The β-ZnS was sintered in a solid-state at 1223 K for 120 min firstly, and then it was homogenized at 1123 K for 60 min. The XRD pattern of artificial sphalerite is shown in Fig. 1.

2.2. Equipment

The pressure-leaching experiment was performed using an FCFD 2-1.0 potential autoclave (the volume of 2000 mL). The body of the autoclave was made of Zr, and the maximum pressure and temperature achievable by the autoclave were 6.0 MPa and 573 K, respectively. A diagrammatic sketch and physical chart of the FCFD 2-1.0 potential high-pressure autoclave are shown in Fig. 2.

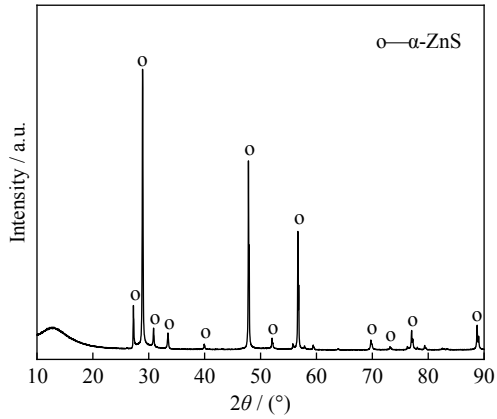

Fig. 1. XRD pattern of artificial sphalerite.

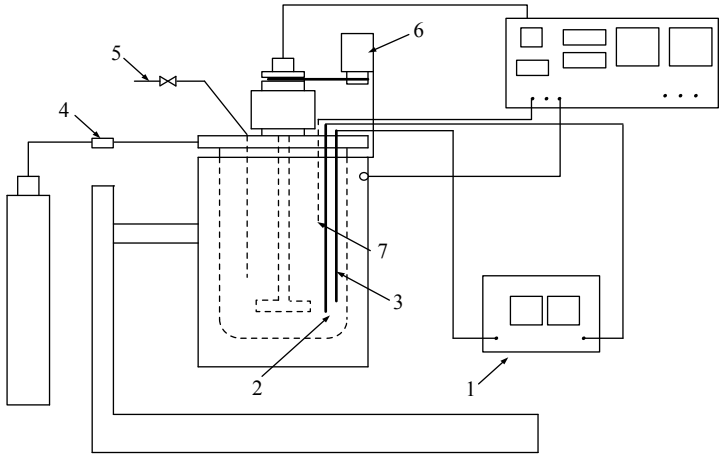

Fig. 2. Potential autoclave. 1—Electrode measuring instrument; 2—Reference electrode; 3—Measuring electrode; 4—Feed inlet; 5—Discharge port; 6—Motor; 7—Thermocouple.

2.3. Leaching experiment

First, 800-mL aqueous solution, 20.0-g artificial sphalerite, and 0.3-g calcium lignosulfonate were added to the potential autoclave and heated to the set temperature. Next, 200-mL sulfuric acid solution and a $CuSO_4$ solution were pressed into the Zr autoclave via O_2; the potential change was recorded by the potentiometer during the reaction.

5-mL slurry was then withdrawn, and the content of Zn was detected by an inductively coupled plasma (ICP) emission spectrometer (Leeman, USA). The experimental flowchart is shown in Fig. 3.

The leaching rate α of valuable elements was calculated as follows:

$$\alpha = \frac{C_1 \times V_1}{m_0 \times x_0} \times 100\% \quad (1)$$

where α is the leaching ratio of zinc (%), C_1 is the concentrate of elements in the leaching solution ($g \cdot L^{-1}$), V_1 is the volume of leaching solution (L), m_0 is the quantity of the sample (g), and x_0 is the mass content of elements in the artificial sphalerite (wt%).

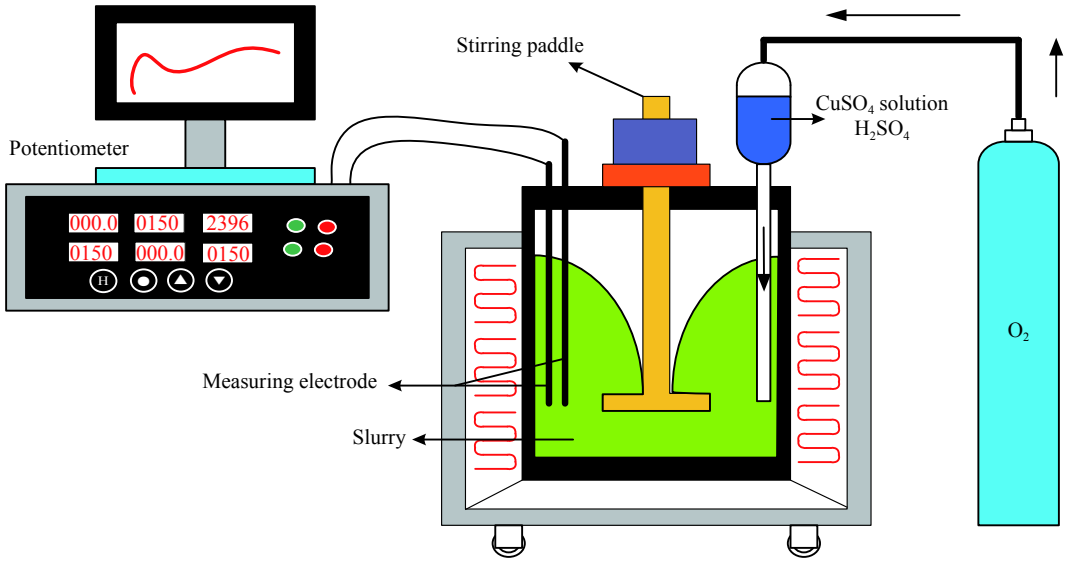

Fig. 3. Flowchart of Cu^{2+} catalyzed in the O_2-pressure acid leaching of the artificial sphalerite.

3. Results and discussion

3.1. Prediction of two different catalytic mechanisms

The O_2-pressure leaching of artificial sphalerite particles in catalytic systems with different cations is shown in Fig. 4. During the pressure leaching of zinc sulfide particles without a cation catalyst, H_2SO_4 first reacted with ZnS, producing H_2S and Zn^{2+}, and H_2S was then oxidized, generating elemental S owing to the $[O]_{solution}$. H^+ was then released, continuing the reaction with ZnS. However, the O dissolution into the leaching solution was very slow, significantly reducing the rate of the leaching reaction.

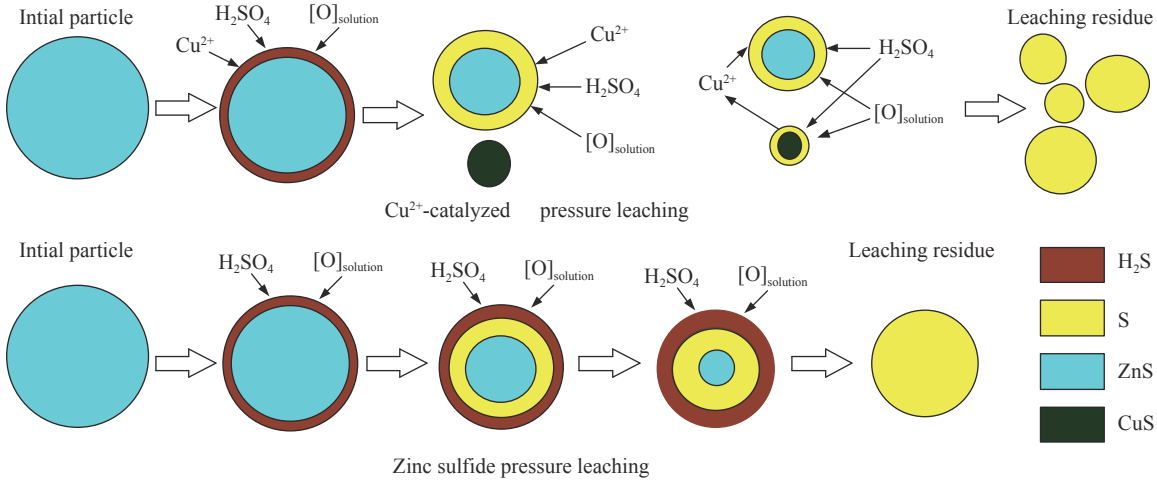

Fig. 4. Schematic of O_2-pressure leaching with artificial sphalerite particles.

$$ZnS + 2H^+ \rightarrow Zn^{2+} + H_2S \quad (2)$$

$$Cu^{2+} + H_2S \rightarrow CuS + 2H^+ \quad (3)$$

$$CuS + 2H^+ + [O]_{solution} \rightarrow Cu^{2+} + S\downarrow + H_2O \quad (4)$$

3.2. Leaching experiment at 363–423 K

3.2.1. Analysis of the catalytic mechanism of Cu^{2+} at 363–423 K

Using artificial sphalerite as a raw material, at the basic conditions with a temperature of 423 K, an H_2SO_4 solution concentration of 140 g/L, an oxygen partial pressure of 1.0 MPa, and a $CuSO_4$ solution concentration of 0.01 mol/L, the Zn extraction and content of Cu^{2+} under different conditions were investigated, as shown in Figs. 5 and 6.

As shown in Figs. 5(b)–5(d), with the increase of temperature, H_2SO_4 concentration, oxygen partial pressure, and leaching time, the leaching rate of Zn exhibited a relatively stable increase. However, as can be seen from Fig. 5(a), the zinc leaching rate during sphalerite oxygen pressure leaching decreases with increasing copper sulfate concentration, and the maximum zinc leaching rate was only 51.04% when the amount of $CuSO_4$ was minimum of 0.01 mol/L, indicating

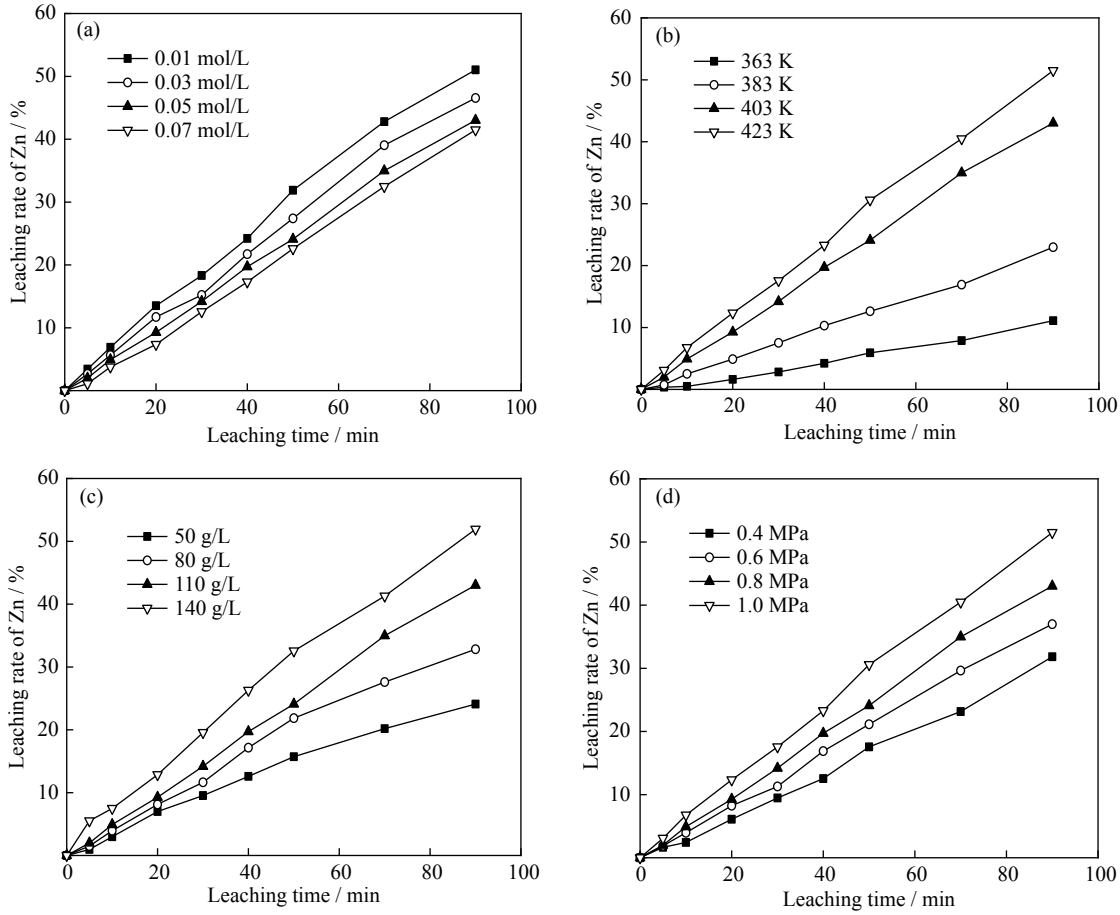

Fig. 5. Effects of different conditions on Zn extraction from the artificial sphalerite: (a) concentrate of $CuSO_4$; (b) temperature; (c) concentrate of H_2SO_4; (d) oxygen partial pressure.

that Cu^{2+} had a poor catalytic effect. This experiment results were inconsistent with the analysis results for the Cu^{2+} catalytic leaching mechanism predicted in Section 3.1.

As shown in Fig. 6, under the different conditions, the Cu^{2+} content in the leaching solution decreased as the leaching time increased. However, most of the Cu still existed in the leaching solution, indicating that the Cu^{2+} reacted with H_2S to a small extent. The CuS deposited on the mineral surface only minimally reacted with the $[O]_{solution}$.

3.2.2. Analysis of system potential at 363–423 K

The relative potential of the O_2-pressure leaching system was investigated at a temperature of 403 K, an H_2SO_4 concentration of 110 g/L, an oxygen partial pressure of 0.8 MPa, and a $CuSO_4$ concentration of 0.05 mol/L. Results are shown in Fig. 7.

As shown in Fig. 7, the potential change in the O_2-pressure leaching system could be divided into the following two regions:

(1) With the addition of sulfuric acid, Cu ions, and O, the rapid increase in the electric potential was mainly due to the addition of a large number of cations, such as Cu^{2+}, H^+, and $[O]_{solution}$. The acid leaching consumption of H^+ reduced the potential.

(2) The potential dropped gently until the end of the leaching experiment, because Cu^{2+} gradually reacted with the H_2S generated by acid leaching, forming CuS. That is, throughout the leaching cycle, the Cu^{2+} and H_2S replacement reaction was continuous and rapid compared with the oxidation rate of CuS, Thus, macroscopically, there appeared to be a continuous decrease in the concentration of Cu^{2+}; that is, the potential of the system decreased continuously.

3.2.3. SEM analysis of leaching slag at 363–423 K

Two experiments were performed at 423 K. In the first, the reaction was stopped immediately after the material was added for 5 min (cooling water was connected, and O_2 pressure was released). In the second, the reaction was completed after the addition of materials for 90 min. The O_2-pressure-leached slag obtained from the two reactions was subjected to SEM analysis to compare the changes in the leaching residue at different reaction times. Results are shown in Figs. 8–10.

As shown in Fig. 9, the mineral surface was still smooth after 5 min of leaching, but pits indicating corrosion were formed on the mineral surface. This indicated that there were not many CuS deposits on the mineral surface at this time; that is, most of the Cu elements still existed in the leaching

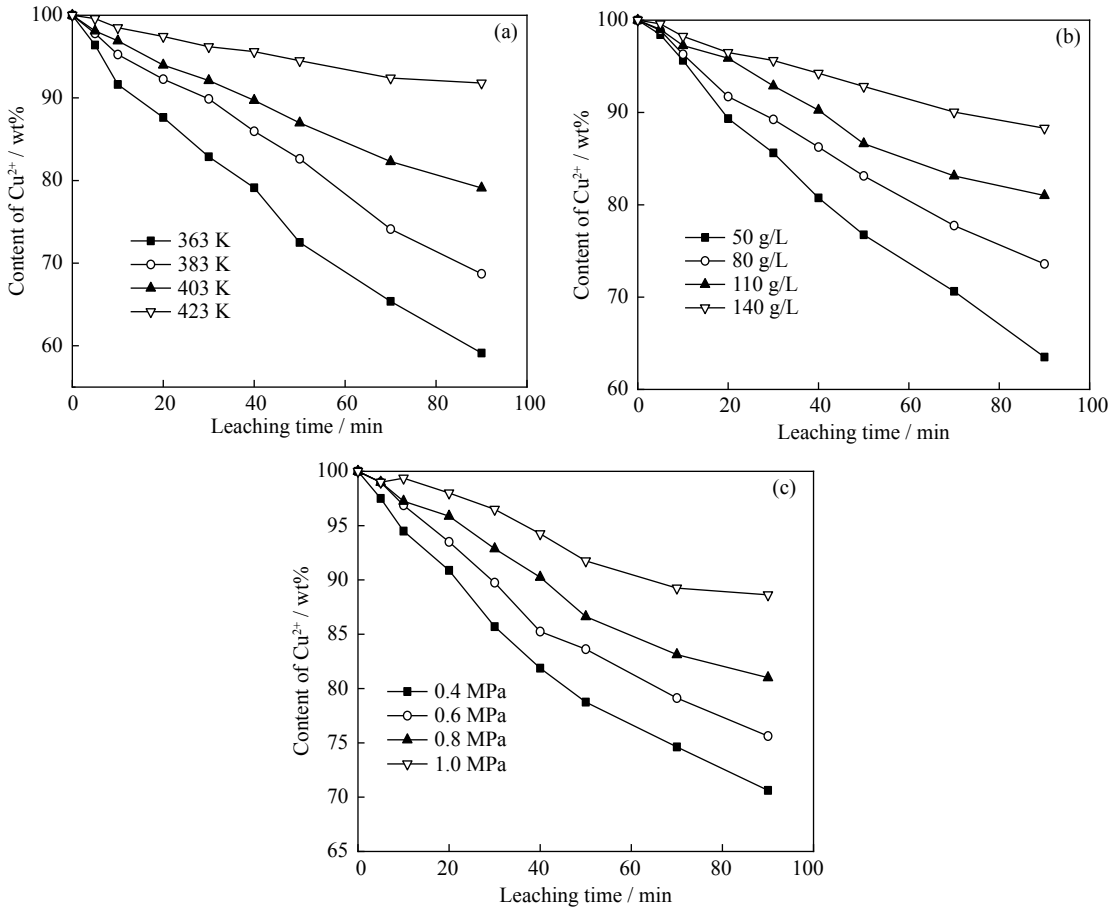

Fig. 6. Effects of different conditions on the Cu^{2+} leached from the artificial sphalerite: (a) temperature; (b) concentrate of H_2SO_4; (c) oxygen partial pressure.

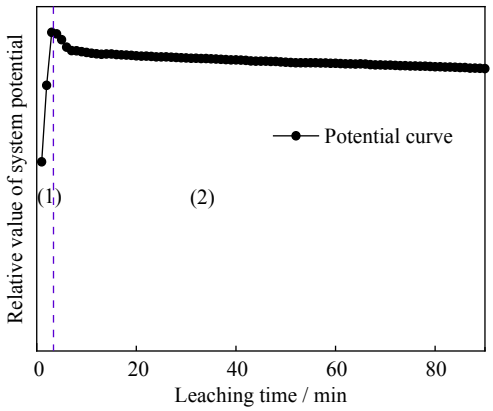

Fig. 7. Potential change in the O_2-pressure leaching process.

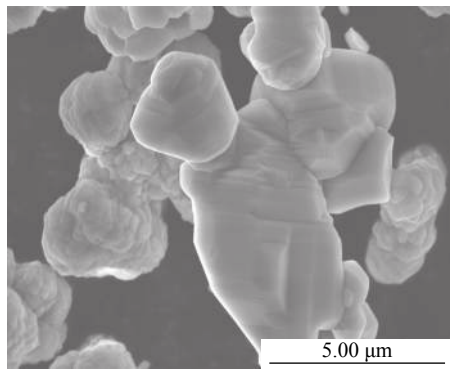

Fig. 8. SEM image showing the morphology of the sphalerite.

solution, and no lattice replacement was achieved through the reaction with H_2S. According to the regional energy-spectrum analysis, most of the leaching residue contained Zn, S, and a few Cu^{2+} deposits.

As shown in Fig. 10, as the leaching time increased, villi deposits were generated on the mineral surface, and the amount of CuS deposited on the mineral surface gradually increased, making the surface rough. Because the CuS had difficulty interacting with the $[O]_{solution}$, once sulfide was formed on the mineral surface, it was almost impossible to reproduce the oxidation to achieve catalyst regeneration. Additionally, the regional energy-spectrum analysis showed that the atomic percentages of Zn, S, and Cu changed after the leaching. In particular, the Cu content increased significantly, indicating that the Cu^{2+} reacted slowly with H_2S as the leaching reaction proceeded. The continuous slow reaction of Cu^{2+} and H_2S and the adhesion and coating on the mineral surface hindered

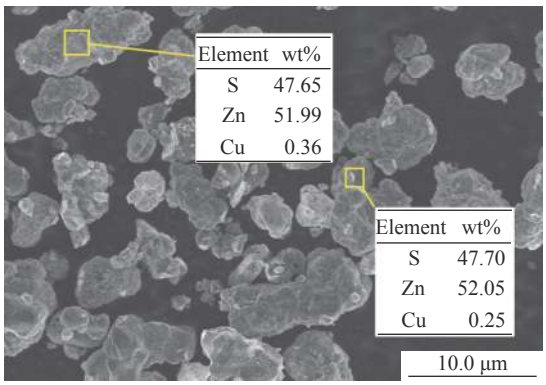

Fig. 9. SEM morphology of the leaching residue with the Cu^{2+} catalytic process (5 min, 423 K).

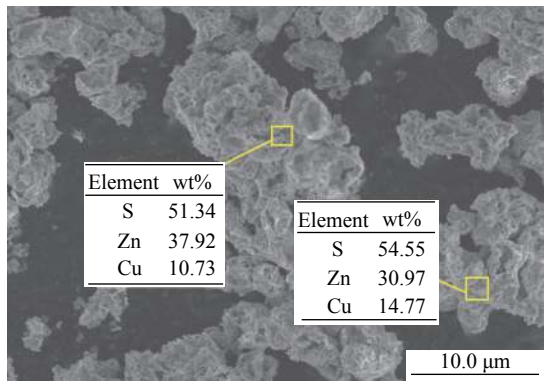

Fig. 10. SEM morphology of the leaching residue with the Cu^{2+} catalytic process (90 min, 423 K).

the leaching reaction.

3.3. Leaching experiment at 423–483 K

3.3.1. Analysis of the catalytic mechanism of Cu^{2+} at 423–483 K

Using artificial sphalerite as a raw material, at the basic conditions with a temperature of 463 K, an H_2SO_4 solution concentration of 110 g/L, an oxygen partial pressure of 0.8 MPa, and a $CuSO_4$ solution concentration of 0.05 mol/L, the Zn extraction under different conditions was investigated, as shown in Figs. 11 and 12.

As shown in Fig. 11, with the increase of temperature, acid concentration, oxygen partial pressure, and leaching time, the leaching rate of Zn increased gradually. The leaching rate of Zn reached 95.71% with a temperature of 463 K, an acidity of 110 g/L, an oxygen partial pressure of 0.8 MPa,

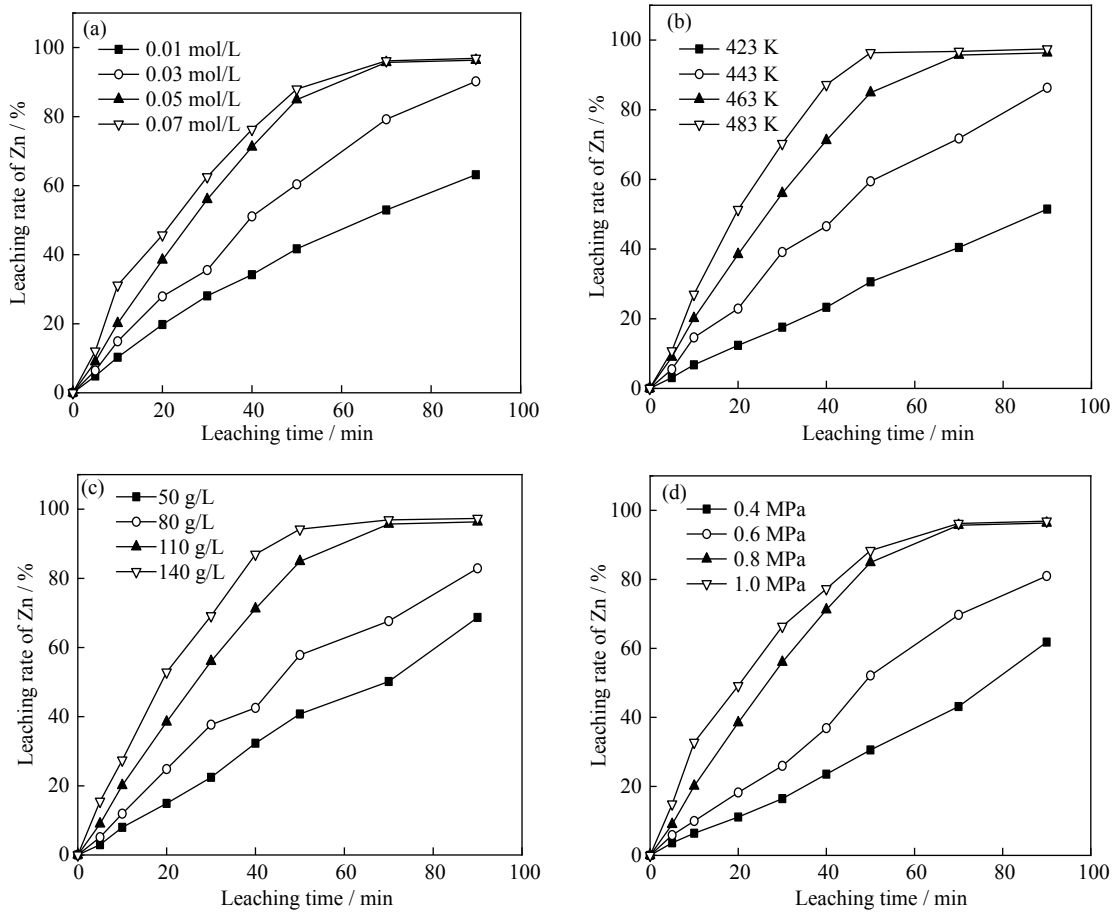

Fig. 11. Effects of different conditions on Zn extraction from the artificial sphalerite: (a) concentrate of $CuSO_4$; (b) temperature; (c) concentrate of H_2SO_4; (d) oxygen partial pressure.

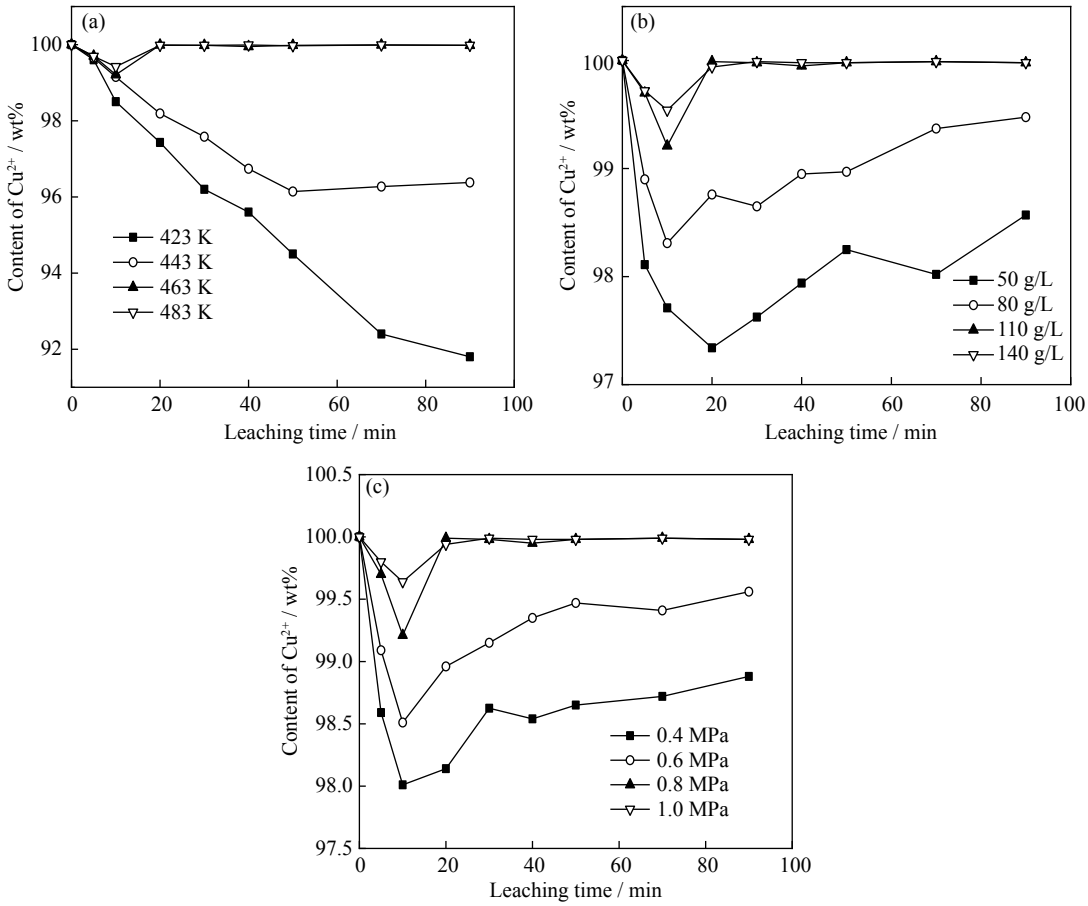

Fig. 12. Effects of different conditions on the Cu^{2+} leached from the artificial sphalerite: (a) temperature; (b) concentrate of H_2SO_4; (c) oxygen partial pressure.

and a $CuSO_4$ solution concentrate of 0.05 mol/L, and the reaction reached equilibrium. As shown in the Fig. 11(a), the Zn leaching rate increased with the amount of Cu added at 463 K, which is in contrast to Fig. 5(a). It was considered that Cu^{2+} had a better catalytic effect when the temperature was ≥ 463 K. Therefore, temperature was an important factor affecting the Cu^{2+} catalytic reaction.

As shown in Fig. 12, when the temperature was ≥463 K, Cu^{2+} content in the leaching solution exhibited a slight decreasing trend within 0–10 min of the leaching time, and then almost entered the leaching solution. When the temperature was 463 K, the sulfuric acid concentration and oxygen partial pressure changed, and this phenomenon, again, occurred. This indicated that the Cu^{2+} participated in the initial stage of the reaction according to Eq. (6). First, it reacted with H_2S, forming CuS. However, this reaction was soon replaced by that in Eq. (7). The CuS deposited on the mineral surface reacted with $[O]_{solution}$ rapidly and released Cu^{2+} for the cyclic reaction. This is consistent with the predicted Cu^{2+} catalytic leaching mechanism in Section 3.1.

3.3.2. Analysis of system potential at 423–483 K

The relative potential of the O_2-pressure leaching system was investigated with a temperature of 463 K, H_2SO_4 concentration of 110 g/L, oxygen partial pressure of 0.8 MPa, and $CuSO_4$ concentration of 0.05 mol. Results are shown in Fig. 13.

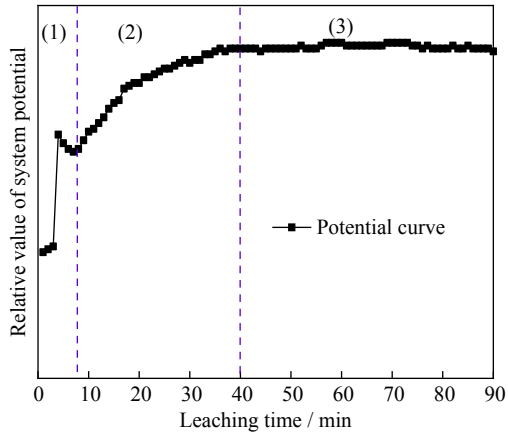

Fig. 13. Potential change in the O_2-pressure leaching process.

In Fig. 13, the curve representing the relative potential of the artificial sphalerite is divided into three areas, and the following observations were made. (1) After the addition of sulfuric acid and O, the system potential increased rapidly and

then decreased. This phenomenon was due to the addition of considerable quantities of H^+, Cu^{2+}, and $[O]_{solution}$, which rapidly increased the potential of the leaching system. Subsequently, the sphalerite in the pyrolysis activation state caused preliminary and rapid acid dissolution. A certain amount of H_2S was generated, which caused the sulfuric acid to be consumed. Additionally, the Cu^{2+} gradually reacted with the H_2S to form CuS, which further reduced the potential. (2) At the beginning of the leaching process, the system potential exhibited a significant overall increasing trend (as shown in Region (2) in Fig. 13) caused by $[O]_{solution}$ and Cu^{2+}. In particular, when the temperature exceeded 463 K, CuS was effectively destroyed by $[O]_{solution}$ and H_2SO_4, and Cu^{2+} was re-released. Thus, the Cu^{2+} and $[O]_{solution}$ improved the elimination and oxidation of the H_2S gas film. (3) During the middle stage of the leaching process, the potential fluctuations were smaller than those in the previous stage because the sphalerite had been consumed; therefore, a larger amount of S^{2-} was oxidized, increasing the system potential. The reduction of the S^{2-} ions gradually weakened the fluctuations in the electric potential, and the curve showed a smooth upward trend. In the final stage of the leaching process, because the basic leaching reaction reached equilibrium and a Zn leaching rate of >90% was achieved in 70 min, no significant change was observed in the potential of the system.

3.3.3. Analysis of SEM of leaching slag at 423–483 K

Two experiments were performed at 463 K, and the experimental conditions were the same as those for the experiment conducted at 423 K (Section 3.2.3). The O_2-pressure leached slag obtained from the two reactions was subjected to SEM analysis to compare the changes in the leaching residue at different reaction times. Results are shown in Figs. 14 and 15.

As shown in Fig. 14, the mineral surface was still relatively smooth after a leaching time of 5 min. According to regional energy-spectrum analysis, CuS was deposited on the mineral surface, indicating that Cu^{2+} and H_2S reacted, yielding lattice replacement, and the increase in temperature was conducive to the reaction between Cu^{2+} and S^{2-}.

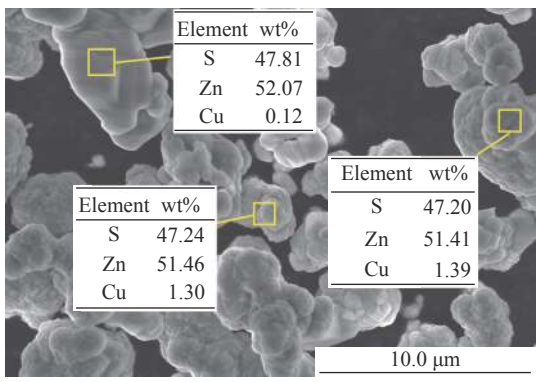

Fig. 14. SEM morphology of the leaching residue with the Cu^{2+} catalytic process (5 min, 463 K).

As shown in Fig. 15, the morphology of the product became a flocculant polymer with increasing leaching time. Owing to the temperature increase, the CuS and sphalerite deposited on the surface of the minerals interacted with $[O]_{solution}$, forming Cu^{2+} and S. The Cu^{2+} and H_2S reacted continuously, and the product was continuously dissolved, yielding the cycle regeneration of Cu^{2+}. Additionally, the regional energy-spectrum analysis showed that the atomic percentages of Zn, S, and Cu were changed after the leaching. In particular, the significant increase in the content of S indicated that with the progress of the leaching reaction, ZnS and CuS were continuously leached out, and Cu^{2+} and $[O]_{solution}$ continued to react with H_2S, yielding elemental S as the final product.

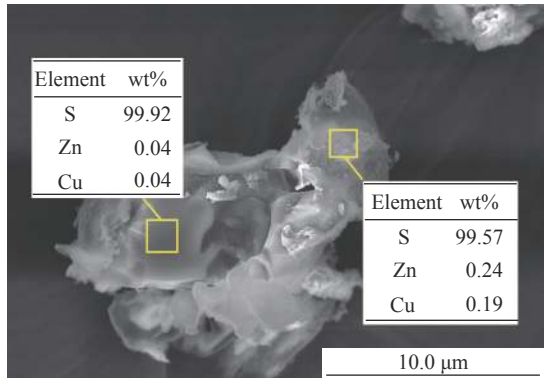

Fig. 15. SEM morphology of the leaching residue with the Cu^{2+} catalytic process (90 min, 463 K).

3.4. Analysis of kinetic equation

In order to determine the control steps of Zn leaching in the Cu catalyst system at different temperature ranges, kinetic experiments were conducted during the leaching process. The kinetic equations [3] were fitted (leaching data from Figs. 5 and 11), and the interface equation was proven to have the best linear correlation by the correlation coefficient. Owusu *et al.* [21–22] found that the dense solid product layer of S was effectively destroyed by adding calcium lignosulfonate in the leaching experiment. Therefore, compared with the other steps, the resistance of the layer could be considered to be relatively small. When the leaching process was controlled by the chemical reaction or by a hybrid control, which is explained in detail later in this section, the equation can be expressed as follows [23]:

$$(1-\alpha)^{1/3} = \frac{K \times C_2^{n_1} \times C_3^{n_2} \times P^{n_3} \times e^{-E/RT}}{r_0 \times \rho} \times t = kt \qquad (5)$$

where k is the synthesis rate constant, K is the rate constant, t is the leaching time (min), C_2 is the concentrate of $CuSO_4$ ($mol \cdot L^{-1}$), C_3 is the concentrate of H_2SO_4 ($g \cdot L^{-1}$), P is the O_2 pressure (MPa), r_0 is the original radius of the particles (μm), T is the reaction temperature (K), ρ is the density of the particles ($kg \cdot m^{-3}$), R = 8.314 $J \cdot mol^{-1} \cdot K^{-1}$ is the universal gas

constant, E is the apparent activation energy ($J \cdot mol^{-1}$), and n_i is the order of the reaction.

3.5. Kinetics of the leaching experiment at 363–423 K

3.5.1. Relationship between Zn leaching rate and reaction temperature

To determine the activation energy in the leaching process, the Zn leaching rates in Fig. 5(b) at different temperatures were plotted and fitted with a regression equation, as shown in Fig. 16. The result shows that the chemical reaction and unreacted shrinkage model had good linear correlation ($[1-(1-\alpha)^{1/3}]$–t).

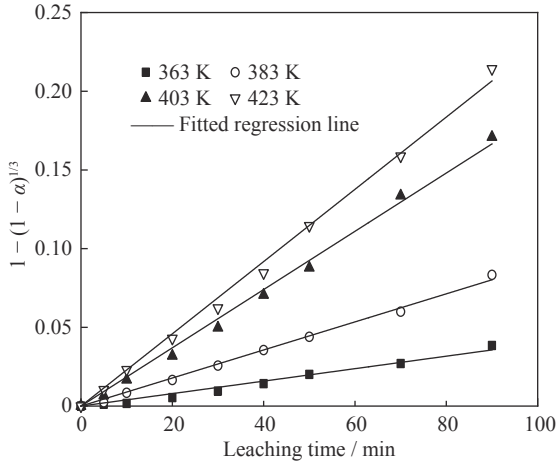

Fig. 16. Plot of the data fitting for the leaching rate of Zn and the leaching time for various temperatures (data from Fig. 5(b)).

Fig. 17 was fitted for the reciprocal of the reaction temperature ($1/T$) versus the natural logarithm of the apparent rate constant ($\ln k$). The apparent activation energy is expressed as follows:

$$k = A_0 e^{-E/RT} \tag{6}$$

where A_0 is the pre-exponential factor.

The activation energy of the Zn leaching at 363–423 K was determined to be 38660 $J \cdot mol^{-1}$, indicating that the process was controlled by surface chemical reactions [23]. The kinetic equation describing the effect of the temperature (363–423 K) on the Zn leaching is as follows:

$$\ln k = 5.06 - 4.65 \times 10^3 / T \tag{7}$$

3.5.2. Relationship between Zn leaching rate and $CuSO_4$ concentration

The addition of $CuSO_4$ had a significant effect on the leaching of Zn. Fig. 18 shows $[1-(1-\alpha)^{1/3}]$ (data from Fig. 5(a)) versus leaching time at different $CuSO_4$ concentrations, and in Fig. 19, these results were used to plot the natural logarithm of the $CuSO_4$ concentration [$\ln c(CuSO_4)$] versus the natural logarithm of the apparent rate constant ($\ln k$). The reaction order of zinc leaching, as calculated from Fig. 19, was

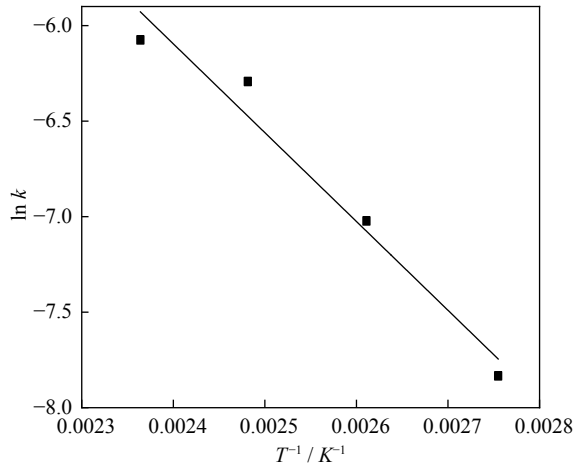

Fig. 17. Relationship between $\ln k$ and T^{-1} for the Zn leaching rates at 363–423 K.

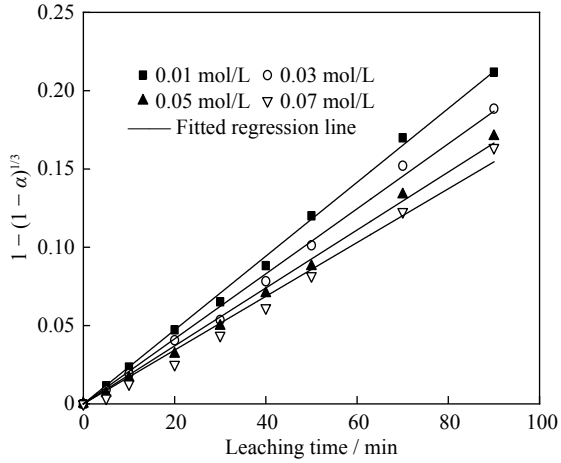

Fig. 18. Plot of $1-(1-\alpha)^{1/3}$ versus t for the leaching rate of Zn at different $CuSO_4$ concentrations (data from Fig. 5(a)).

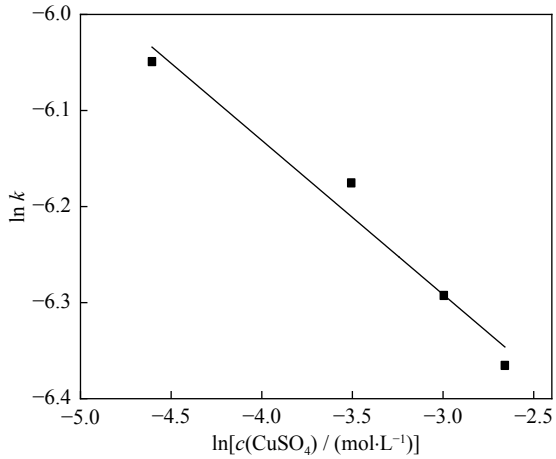

Fig. 19. Relationship between $\ln k$ and $\ln c(CuSO_4)$ for Zn leaching.

−0.16, indicating that the increase in the Cu^{2+} concentration hindered the leaching reaction [3]. The kinetic equation de-

scribing the effect of the $CuSO_4$ concentration on the Zn leaching rate is as follows:

$$\ln k = -6.77 - 0.16 \ln c(CuSO_4) \quad (8)$$

3.5.3. Relationship between Zn leaching rate and H_2SO_4 concentration

Fig. 20 shows $[1-(1-\alpha)^{1/3}]$ (data from Fig. 5(c)) versus leaching time at different H_2SO_4 concentrations, and Fig. 21, the relationship between the natural log of the apparent rate constant ($\ln k$) and the natural log of the concentrate of H_2SO_4 [$\ln c(H_2SO_4)$]. The reaction order for zinc leaching, as calculated from Fig. 21, was 0.8. Thus, the kinetic equation describing the effect of the H_2SO_4 concentration on the Zn leaching rate is as follows:

$$\ln k = -10.04 + 0.8 \ln c(H_2SO_4) \quad (9)$$

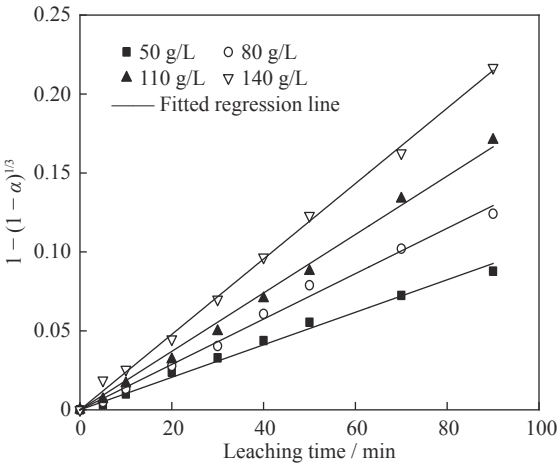

Fig. 20. Plot of $1-(1-\alpha)^{1/3}$ versus t for the leaching rate of Zn at different H_2SO_4 concentrations (data from Fig. 5(c)).

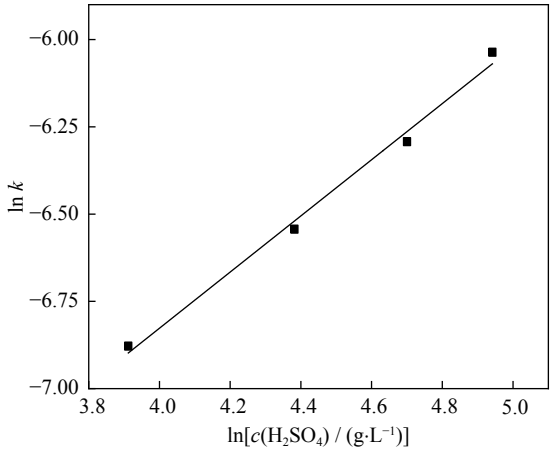

Fig. 21. Relationship between $\ln k$ and $\ln c(H_2SO_4)$ for Zn leaching.

3.5.4. Relationship between Zn leaching rate and oxygen partial pressure

Fig. 22 shows $[1-(1-\alpha)^{1/3}]$ (Data from Fig. 5(d)) versus leaching time at oxygen partial pressure, and Fig. 23 shows the natural logarithm of the natural logarithm of the oxygen partial pressure ($\ln P_{O2}$) and the apparent rate constant ($\ln k$). The reaction order for Zn leaching, as calculated from Fig. 23, was 0.66. Thus, the kinetic equation describing the effect of the oxygen partial pressure on the Zn leaching rate is as follows:

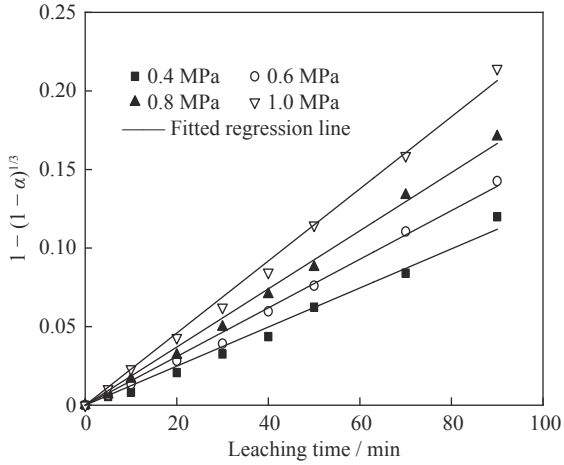

Fig. 22. Plot of $1-(1-\alpha)^{1/3}$ versus t for the leaching rate of Zn at different oxygen partial pressures (data from Fig. 5(d)).

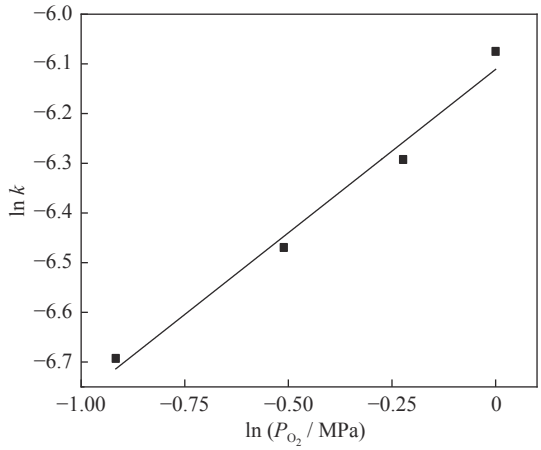

Fig. 23. Relationship between $\ln k$ and $\ln P_{O_2}$ for Zn leaching.

$$\ln k = -6.11 + 0.66 \ln P_{O_2} \quad (10)$$

3.6. Kinetics of the leaching experiment at 423–483 K

3.6.1. Relationship between Zn leaching rate and reaction temperature

To determine the activation energy in the leaching process, the Zn leaching rates in Fig. 11(b) at different temperatures were plotted and fitted with a regression equation, as shown in Fig. 24.

According to the fitting results in Fig. 24, Fig. 25 shows the natural logarithm of the apparent rate constant ($\ln k$) versus the reciprocal of the reaction temperature ($1/T$). The apparent activation energy was calculated by Eq. (6).

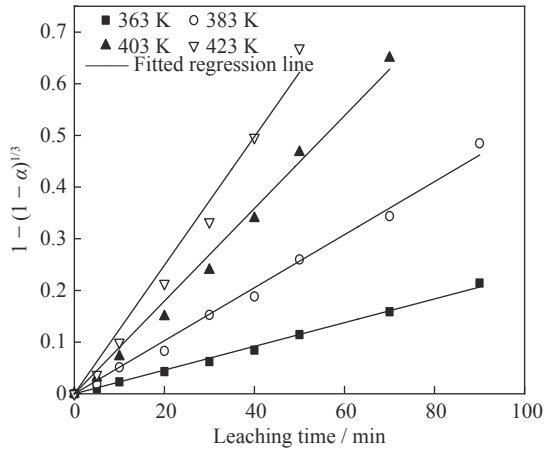

Fig. 24. Plot of the data fitting for the leaching rate of Zn and the leaching time for various temperatures (data from Fig. 11(b)).

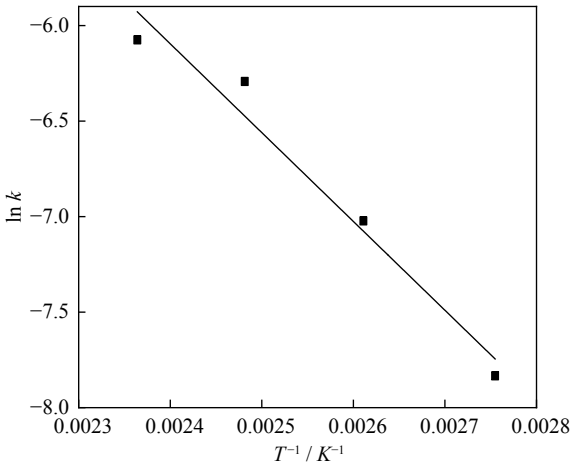

Fig. 25. Relationship between ln k and T^{-1} for the Zn leaching rate at 423–483 K.

The activation energy of the Zn leaching rates at 423–483 K was determined to be 36249 J·mol^{-1}, indicating that the process was controlled by surface chemical reactions [23]. The kinetic equation describing the effect of the temperature (423–483 K) on the Zn leaching rate is as follows:

$$\ln k = 6.01 - 4.36 \times 10^3 / T \quad (11)$$

3.6.2. Relationship between Zn leaching rate and $CuSO_4$ concentration

The addition of $CuSO_4$ had a significant effect on the leaching of Zn. Fig. 26 shows $[1-(1-\alpha)^{1/3}]$ (data from Fig. 11(a)) versus leaching time at different $CuSO_4$ concentrations, and in Fig. 27, these results are used to plot the natural logarithm of the $CuSO_4$ concentration [ln $c(CuSO_4)$] versus the natural logarithm of the apparent rate constant (ln k). The reaction order for zinc leaching, as calculated from Fig. 27, was 0.59, indicating that the increase in the Cu^{2+} concentration promoting the leaching reaction. The kinetic equation describing the effect of the $CuSO_4$ concentration on the Zn leaching rate is as follows.

$$\ln k = -3.04 + 0.59 \ln c(CuSO_4) \quad (12)$$

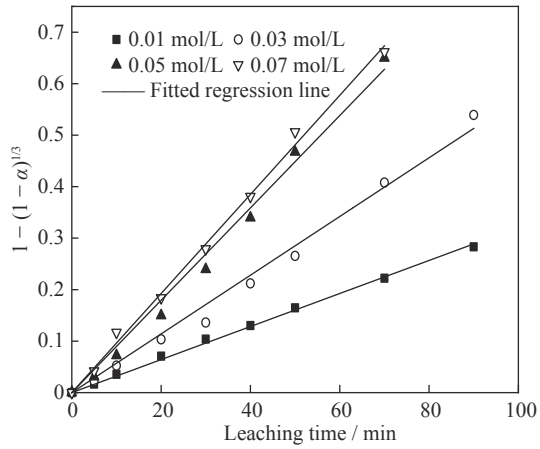

Fig. 26. Plot of $1-(1-\alpha)^{1/3}$ versus t for the leaching rate of Zn at different $CuSO_4$ concentrations (data from Fig. 11(a)).

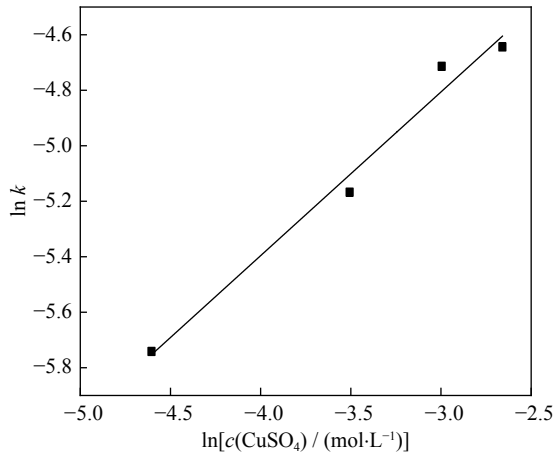

Fig. 27. Relationship between ln k and ln $c(CuSO_4)$ for Zn leaching.

3.6.3. Relationship between Zn leaching rate and H_2SO_4 concentration

Fig. 28 shows $[1-(1-\alpha)^{1/3}]$ (data from Fig. 11(c)) versus time at different H_2SO_4 concentrations, and in Fig. 29, these results were used to plot the natural logarithm of the H_2SO_4 concentration [ln $c(H_2SO_4)$] versus the natural logarithm of the apparent rate constant (ln k). The reaction order for Zn leaching, as calculated from Fig. 29, was 0.8. Thus, the kinetic equation describing the effect of the H_2SO_4 concentration on the Zn leaching rate is as follows:

$$\ln k = -10.93 + 1.31 \ln c(H_2SO_4) \quad (13)$$

3.6.4. Relationship between Zn leaching rate and oxygen partial pressure

Fig. 30 shows $[1-(1-\alpha)^{1/3}]$ (data from Fig. 11(d)) versus leaching time at different partial pressures of O_2, and in Fig. 31, the natural log of the oxygen partial pressure (ln

P_{O2}) and the natural log of the apparent rate constant (ln k) are plotted. The reaction order for Zn leaching, as calculated from Fig. 31, was 1.54. Thus, the kinetic equation describing the effect of the oxygen partial pressure on the Zn leaching rate is as follows:

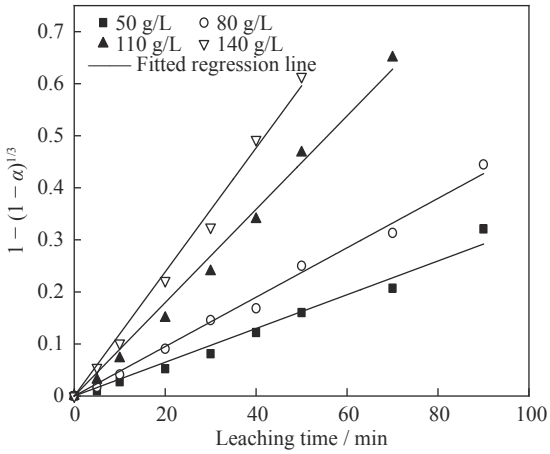

Fig. 28. Plot of $1-(1-\alpha)^{1/3}$ versus t for the leaching rate of Zn at different H_2SO_4 concentrations (data from Fig. 11(c)).

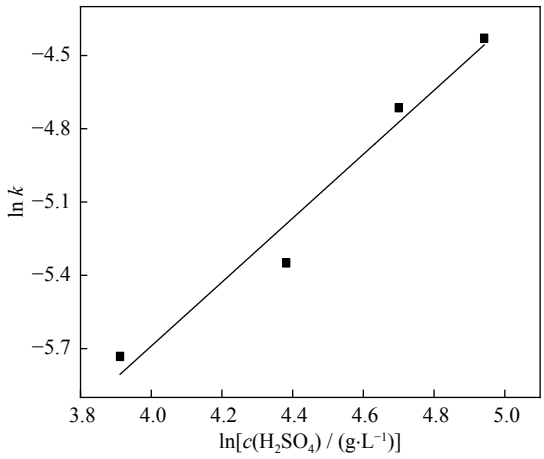

Fig. 29. Relationship between ln k and ln $c(H_2SO_4)$ for Zn leaching.

$$\ln k = -4.54 + 1.54 \ln P_{O_2} \tag{14}$$

3.7. Establishment of kinetic equation

According to Eq. (5), the kinetic equation can be expressed as follows:

$$1-(1-\alpha)^{1/3} = K \times c(CuSO_4)^{n_1} \times c(H_2SO_4)^{n_2} \times P_{O_2}^{n_3} \times e^{-E/RT} \times t \tag{15}$$

where K is the pre-exponential factor.

The relationships between $[1-(1-\alpha)^{1/3}]$ and $K_0 \times c(CuSO_4)^{n_1} \times c(H_2SO_4)^{n_2} \times P_{O_2}^{n_3} \times e^{-E/RT} \times t$ for the artificial sphalerite O_2-pressure leaching at 363–423 and 423–483 K are shown in Fig. 32. Although the points in the plot show scattering, the straight lines could be fitted to the data with a correlation coefficient of > 0.97. Thus, according to Fig. 32, K_0 was determined to be 0.053 and 0.028 for 363–423 and 423–483 K, respectively.

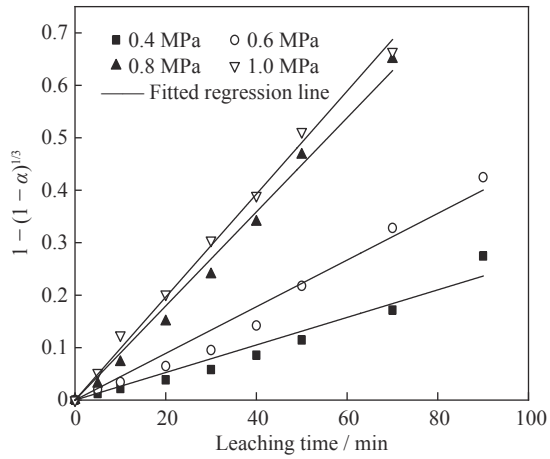

Fig. 30. Plot of $1-(1-\alpha)^{1/3}$ versus t for the leaching rate of Zn at different oxygen partial pressures (data from Fig. 11(d)).

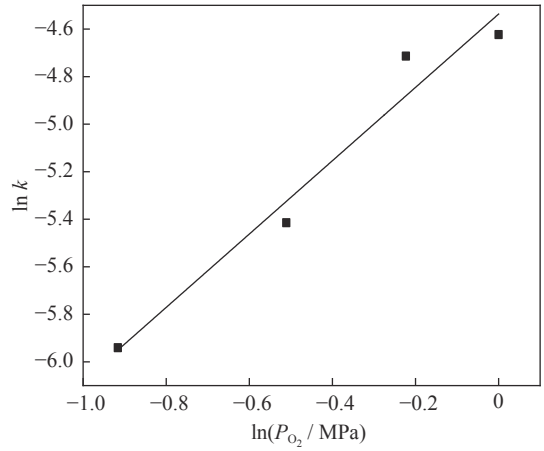

Fig. 31. Relationship between ln k and ln P_{O_2} for Zn leaching.

According to the activation energy, reaction order, the kinetic equations of the artificial sphalerite O_2-pressure leaching at 363–423 and 423–483 K could be expressed as Eqs. (16) and (17), respectively:

$$1-(1-\alpha)^{1/3} = 0.053 \times c(CuSO_4)^{-0.16} \times c(H_2SO_4)^{0.80} \times P_{O_2}^{0.66} \times e^{-38660/RT} \times t \tag{16}$$

$$1-(1-\alpha)^{1/3} = 0.028 \times c(CuSO_4)^{0.59} \times c(H_2SO_4)^{1.31} \times P_{O_2}^{1.54} \times e^{-36249/RT} \times t \tag{17}$$

4. Conclusions

In this paper, the catalytic mechanism of Cu^{2+} in the oxygen pressure acid leaching process of artificial sphalerite was studied, and the following conclusions can be drawn.

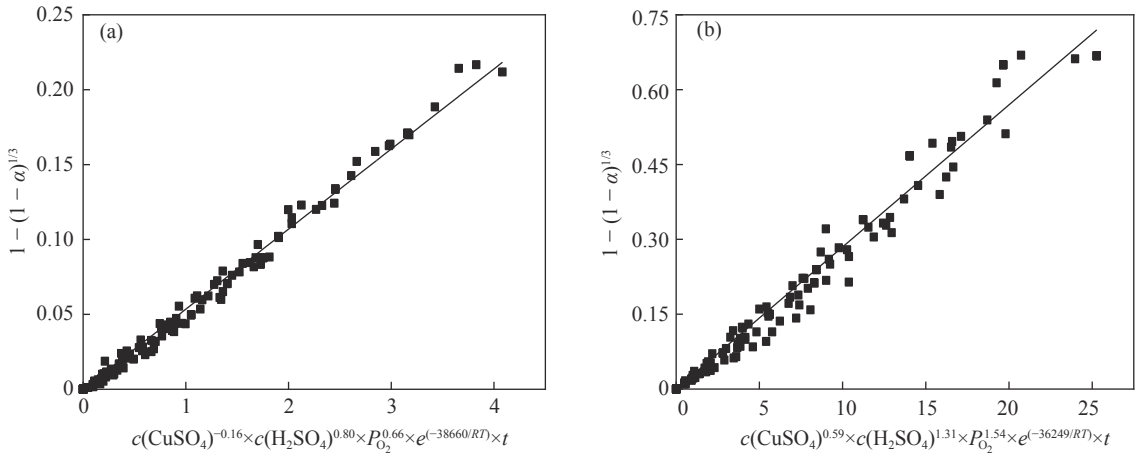

Fig. 32. Relationships between $1-(1-\alpha)^{1/3}$ and $K\times c(CuSO_4)^{n_1}\times c(H_2SO_4)^{n_2}\times P_{O_2}^{n_3}\times e^{-E/RT}\times t$ for the artificial sphalerite O_2-pressure leaching at (a) 363–423 K and (b) 423–483 K.

(1) The zinc leaching behavior of artificial sphalerite in two different temperature ranges of 363–423 and 423–483 K was different. At 363–423 K, the zinc leaching efficiency gradually increased with the increase of temperature, acidity, and oxygen partial pressure, but decreased with the increase of $CuSO_4$ concentration, the highest leaching rate was only 51.04%. However, the zinc leaching efficiency increased with increasing temperature, acidity, oxygen partial pressure, and $CuSO_4$ concentration at 423–483 K, and the zinc leaching rate can reach 95.71%.

(2) When the temperature was lower than 423 K, SEM–EDS showed that with the increase of leaching time, copper content on mineral surface gradually increased and villous sediments were formed. It was because the Cu^{2+} react with H_2S generates CuS, and deposited on the surface of the mineral to hinder the leaching reaction, at this time, with the increased of leaching time, the system potential gradually decreases.When the temperature exceeds 423 K, CuS on the surface of the mineral reacts with $[O]_{solution}$ to form Cu^{2+} and S, Cu^{2+} can act as a catalyst to promote zinc ion leaching. At this time, with the increase of leaching time, the system potential shows a steady rise trend.

(3) The activation energy of the O_2-pressure acid leaching of the artificial sphalerite at 363–423 and 423–483 K was 38660 and 36230 $J\cdot mol^{-1}$, respectively. The apparent reaction orders of Cu^{2+}, sulfuric acid, and oxygen partial pressure at 368–432 K were determined to be 0.6, 0.8, and 0.66, respectively, and at 423–483 K were 0.59, 1.31, and 1.54, respectively. Finally, the kinetic equation for fitting the results was formulated.

Acknowledgements

This work was financially supported by the Joint Funds of the National Natural Science Foundation of China (Nos. 51804136, U1402271, 51764016), Jiangxi Province Nature Science Foundation, China (No. 20181BAB216017), Jiangxi Science and Technology Landing Project, China (No. KJLD13046), and Research Fund Program of State Key Laboratory of Rare Metals Separaten and Comprehensive Utilization, Guangzhou, China (No. GK-201803).

References

[1] T.J. Harvey, W. Tai Yen, and J.G. Paterson, A kinetic investigation into the pressure oxidation of sphalerite from a complex concentrate, *Miner. Eng.*, 6(1993), No. 8-10, p. 949.

[2] R.J. Jan, M.T. Hepworth, and V.G. Fox, A kinetic study on the pressure leaching of sphalerite, *Metall. Mater. Trans. B*, 7(1976), No. 3, p. 353.

[3] L. Tian, Y. Liu, T.A. Zhang, G.Z. Lv, S. Zhou, and G.Q. Zhang, Kinetics of indium dissolution from marmatite with high indium content in pressure acid leaching, *Rare Met.*, 36(2017), No. 1, p. 69.

[4] L. Tian, Y. Liu, J.J Tang, G.Z. Lü, and T.A. Zhang, Variation law of gas holdup in an autoclave during the pressure leaching process by using a mixed-flow agitator, *Int. J. Miner. Metall. Mater.*, 24(2017), No. 8, p. 876.

[5] F.E.D.L. Santos, R.E. Rivera-Santillan, M. Talavera-Ortega, and F. Bautista, Catalytic and galvanic effects of pyrite on ferric leaching of sphalerite, *Hydrometallurgy*, 163(2016), p. 167.

[6] J.S. Niederkorn, Kinetic study on catalytic leaching of sphalerite, *JOM*, 37(1985), No. 7, p. 53.

[7] Z.X. Liu, Z.L. Yin, H.P. Hu, and Q.Y. Chen, Catalytic-oxidative leaching of low-grade complex zinc ore by Cu(II) ions produced from copper ore in ammonia-ammonium sulfate solution, *Metall. Mater. Trans. B*, 43(2012), No. 5, p. 1019.

[8] S. Karimi, A. Ghahreman, F. Rashchi, and J. Moghaddam, The mechanism of electrochemical dissolution of sphalerite in sulfuric acid media, *Electrochim. Acta*, 253(2017), p. 47.

[9] F. Habashi, Dissolution of minerals and hydrometallurgical processes, *Naturwissenschaften*, 70(1983), No. 8, p. 403.

[10] Y. Li, N. Kawashima, J. Li, A.P. Chandra, and A.R. Gerson, A review of the structure, and fundamental mechanisms and kinetics of the leaching of chalcopyrite, *Adv. Colloid Interface Sci.*, 197-198(2013), p. 1.

[11] J. Liu, S.M. Wen, Y.J. Wang, J.S. Deng, and X.M. Chen, Trans-

ition state search study on the migraten of Cu absorbed on the S sites of sphalerite (110) surface, *Int. J. Miner. Process.*, 147(2016), p. 28.

[12] J. Lorenzo-Tallafigo, N. Iglesias-Gonzalez, R. Romero, A. Mazuelos, and F. Carranza, Ferric leaching of the sphalerite contained in a bulk concentrate: Kinetic study, *Miner. Eng.*, 125(2018), p. 50.

[13] V.V. Zhukov, A. Laari, M. Lampinen, and T. Koiranen, A mechanistic kinetic model for direct pressure leaching of iron containing sphalerite concentrate, *Chem. Eng. Res. Des.*, 118(2017), p. 131.

[14] S.F. Wang, Z. Fang, S. Long, and Y.G. Chen, Electrogenerative simultaneously leaching of sulfide minerals and MnO_2, *Nonferrous Met.*, 56(2004), No. 1, p. 56.

[15] S.F. Wang, L. Xiao, Z. Fang, G.Z. Qiu, and C.X. Wang, Electrogenerative leaching for sphalerite-MnO_2 in the presence of Acidithiobacillus thiooxidans, *Trans. Nonferrous Met. Soc. China*, 20(2010), No. supplement 1, p. s21.

[16] M.E. Escudero, F. Gonzalez, M.L. Blázquez, A. Ballester, and C. Gómez, The catalytic effect of some cations on the biological leaching of a Spanish complex sulphide, *Hydrometallurgy*, 34(1993), No. 2, p. 151.

[17] C.M. Ai, P.P. Sun, A.X. Wu, X. Chen, and C. Liu, Accelerating leaching of copper ore with surfactant and the analysis of reaction kinetics, *Int. J. Miner. Metall. Mater.*, 26(2019), No. 3, p. 274.

[18] E.M. Córdoba, J.A. Muñoz, M.L. Blázquez, F. González, and A. Ballester, Leaching of chalcopyrite with ferric ion. Part III: Effect of redox potential on the silver-catalyzed process, *Hydrometallurgy*, 93(2008), No. 3-4, p. 97.

[19] M.K. Ghosh, R.P. Das, and A.K. Biswas, Oxidative ammonia leaching of sphalerite.Part II: Cu(II)-catalyzed kinetics, *Int. J. Miner. Process.*, 70(2003), No. 1-4, p. 221.

[20] A.Ballester, F.González, M.L. Blázquez, and J.L. Mier, The influence of various ions in the bioleaching of metal sulphides, *Hydrometallurgy*, 23(1990), No. 2-3, p. 221.

[21] G. Owusu, D.B. Dreisinger, and E. Peters, Effect of surfactants on zinc and iron dissolution rates during oxidative leaching of sphalerite, *Hydrometallurgy*, 38(1995), No. 3, p. 315.

[22] G. Owusu, D.B. Dreisinger, and E. Peters, Interfacial effects of surface-active agents under zinc pressure leach conditions, *Metall. Mater. Trans. B*, 26(1995), No. 1, p. 5.

[23] L. Tian, Z.F. Xu, L.J. Chen, Y. Liu, and T.A. Zhang, Study on oxygen gas holdup and kinetics using various types of paddles during marmatite leaching process, *Hydrometallurgy*, 180(2018), p. 158.